Contents lists available at ScienceDirect

Palaeogeography, Palaeoclimatology, Palaeoecology

journal homepage: www.elsevier.com/locate/palaeo

A multi-proxy approach to constrain reducing conditions in the Baltic Basin during the late Silurian Lau carbon isotope excursion

Chelsie N. Bowman [a,b,*], Theodore R. Them II [c], Marisa D. Knight [c], Dimitri Kaljo [d], Mats E. Eriksson [e], Olle Hints [d], Tõnu Martma [d], Jeremy D. Owens [a], Seth A. Young [a]

[a] Department of Earth, Ocean & Atmospheric Sciences, National High Magnetic Field Laboratory, Florida State University, Tallahassee, FL 32306, USA
[b] Department of Geosciences, Pennsylvania State University, State College, PA 16802, USA
[c] Department of Geology and Environmental Geosciences, College of Charleston, Charleston, SC 29424, USA
[d] Department of Geology, Tallinn University of Technology, Ehitajate tee 5, 19086 Tallinn, Estonia
[e] Department of Geology, Lund University, Sölvegatan 12, SE-223 62 Lund, Sweden

ARTICLE INFO

Editor: Thomas Algeo

Keywords:
Trace metals
Iron speciation
Iodine
Mercury
Lau/Kozlowskii extinction

ABSTRACT

The Silurian was a dynamic time characterized by significant climatic and sea level changes, biotic crises, and carbon cycle volatility. The largest magnitude perturbation to the Silurian global carbon cycle was the mid-Ludfordian carbon isotope excursion, termed the Lau CIE, which was coincident with the Lau/Kozlowskii extinction (LKE). Much of the published research on the late Silurian has described changes in the biotic record and global marine redox conditions. Limited work has been done, however, to elucidate the variability in local paleo-redox conditions. Here, we use a suite of paleo-redox proxies to examine a shallow shelf carbonate succession from Gotland, Sweden, and a deep shelf clastic sequence from Latvia. Low iodine-to-calcium ratios from the carbonate succession suggest an anoxic water column, or significant exchange with nearby reducing water masses. Iron speciation data and moderate trace metal enrichments suggest that the sediments of the deeper shelf were deposited in an oxygen minimum zone with a denitrifying water column before and during the LKE with sulfidic conditions limited to the sediment porewaters. After the extinction, a relative depletion in trace metal concentrations (V, Hg, U, Mo) suggest that water column conditions were locally less reducing. The depletion in trace metal concentrations is coeval with previously reported global increases in anoxia and euxinia after the LKE and, thus, potentially could have resulted from a global drawdown in trace metals overprinted upon the local record of paleo-redox change.

1. Introduction

One of the largest carbon isotope excursions of the Phanerozoic was the late Silurian (Ludfordian Stage) Lau CIE, with peak excursion magnitude averaging between +5 to +9‰ (Munnecke et al., 2003; see Calner, 2008 for review; Saltzman and Thomas, 2012). The Lau CIE was accompanied by the most severe extinction event of the Silurian and tenth most severe extinction in Earth history, the Lau/Kozlowskii extinction (LKE), named for the asynchronous extinctions of conodonts and graptolites (Jeppsson, 1990; Koren, 1993; Urbanek, 2003; Bond and Grasby, 2017; compiled in Bowman et al., 2019). The onset of the LKE slightly predates the Lau CIE and it has been suggested for almost two decades that both the extinction event and the carbon cycle perturbation were the result of an expansion of reducing conditions in the global ocean (e.g., Munnecke et al., 2003; Stricanne et al., 2006). Recent studies of the Ludfordian strata of Baltica (Bowman et al., 2019; del Rey et al., 2020) and southern Laurentia (Bowman et al., 2020) have used a variety of geochemical and paleontological tools to test this hypothesis. In the deep-water shales and marls of the Baltic Basin (Latvia), a positive excursion in thallium isotopes was recorded coincident with the onset of the LKE (Bowman et al., 2019). This excursion suggests that the first extinction stages of the LKE, in benthic and nektonic fauna, were caused by a global expansion of bottom-water anoxia (Bowman et al., 2019). This is supported by a study by del Rey et al. (2020) that applied

* Corresponding author.
E-mail addresses: cvb5950@psu.edu (C.N. Bowman), themtr@cofc.edu (T.R. Them), knightmd1@g.cofc.edu (M.D. Knight), dimitri.kaljo@taltech.ee (D. Kaljo), mats.eriksson@geol.lu.se (M.E. Eriksson), olle.hints@taltech.ee (O. Hints), tonu.martma@taltech.ee (T. Martma), jdowens@fsu.edu (J.D. Owens), sayoung2@fsu.edu (S.A. Young).

https://doi.org/10.1016/j.palaeo.2021.110624
Received 18 May 2021; Received in revised form 17 August 2021; Accepted 18 August 2021

uranium isotopes using brachiopod shells in the shallow-water carbonates of the Baltic Basin (Gotland, Sweden). This study reports uranium isotope values more negative than that of the modern ocean, suggesting that the global Ludfordian oceans had a greater extent of anoxic water masses. No uranium isotope excursion, however, has thus far been recorded, likely because their sampled interval corresponds primarily to before and during the LKE event (early – middle Ludfordian) when global marine redox conditions were consistently reducing, with the initial deoxygenation and later recovery not captured in this temporally incomplete record. The expansion of reducing conditions in the Ludfordian oceans has been further elucidated by records of positive excursions in carbonate-associated sulfate (CAS) sulfur isotopes in carbonate strata from Baltica (Gotland; Bowman et al., 2019) and southern Laurentia (Tennessee, USA; Bowman et al., 2020). The positive excursion in CAS sulfur isotopes suggests a notable increase in the burial of pyrite in the global oceans, likely due to an expansion of euxinic conditions (anoxia with free sulfide) in the water column and/or sulfidic conditions in sediment porewaters (Bowman et al., 2019, 2020). This subsequent expansion in the severity and/or extent of reducing conditions in the global ocean was coincident with the onset of the Lau CIE and likely related to the later extinctions in planktic fauna during the LKE (Bowman et al., 2019).

These fluctuations in paleo-redox conditions likely triggered changes in the Ludfordian biotic record, and the resultant interval of enhanced carbon burial (i.e., initiation of the Lau CIE). The redox variability is discussed as an expansion of the fraction of reducing conditions in the global oceans, rather than the entire global oceans becoming anoxic or euxinic. Previous studies have used geochemical box modeling to estimate the extent of marine euxinia during comparable events in the Mesozoic and Paleozoic, finding that increases of only ~5–10% of the global seafloor are necessary to drive geochemical perturbations like those observed in the Ludfordian (e.g., Gill et al., 2011; Owens et al., 2013; Dickson et al., 2016; Lau et al., 2016; Zhang et al., 2018; Young et al., 2019). A few studies have parsed out the extent of anoxic vs. euxinic environments, but in all such cases, the extent of reducing bottom waters was still only a fraction of the total global seafloor. Detailed local redox conditions in the Ludfordian have only been documented along the carbonate shelf of the southern Laurentian margin, where Bowman et al. (2020) identified variations in local water-column and sediment porewater redox, based on I/Ca ratios and pyrite sulfur isotopes, that coincided with the Lau CIE and changes in local biotic records (e.g., carbonate microfacies). Few constraints exist for local to regional redox dynamics through the Lau CIE and LKE intervals in the Baltic Basin, however, despite this region having the most comprehensive documentation of changes in the biotic record and global ocean redox state.

We present new iodine-to-calcium ratio data from the shallow shelf carbonates of Gotland, Sweden. As most of the commonly used local paleo-redox proxies are exclusively used in organic-rich shales and mudstones, I/Ca values offer important insight into the local redox conditions of shallow carbonate shelf environments. We also show new iron speciation and trace element (Mn, V, Hg, U, Mo) concentration data from the deep shelf shales and marls of Latvia. Variations in authigenic trace metal concentrations can be interpreted as indicators of either local or global redox change, contingent upon local redox conditions. As such, we have used Fe speciation to offer an independent constraint on local paleo-redox. Altogether, these proxies are used to assess changes in the local water column and sediment porewater redox conditions in the Baltic Basin through the Lau CIE and the Lau/Kozlowskii extinction intervals. Key information and additional references for each of these local paleo-redox proxies are summarized in Table 1. Herein, suboxic refers to low, but non-zero, oxygen concentrations; anoxic refers to oxygen concentrations that are effectively zero; euxinic refers to anoxic water column conditions with free hydrogen sulfide. Local paleo-redox conditions are first discussed in terms of this more conservative terminology before using comparisons to modern oxygen minimum zones (OMZ) to more specifically define water column and sediment porewater redox conditions.

2. Geologic setting and biostratigraphy

The late Silurian Baltic Basin was a tropical, epicratonic seaway on the southern margin of the paleocontinent Baltica (e.g. Eriksson and Calner, 2008; Fig. 1). This basin was dominated by rimmed carbonate shelves with parallel facies belts ranging from lagoonal facies in the north to deep shelf facies in the south, deepening towards the Rheic Ocean (Kaljo et al., 1997; Eriksson and Calner, 2008). The Baltic Basin was well connected to the Rheic Ocean during the Ludfordian despite the ongoing Caledonian Orogeny as Laurentia and Baltica collided – though the orogenic activity did result in higher subsidence and sedimentation rates in the deepest parts of the Baltic Basin (Kozłowski and Munnecke, 2010; Kozłowski and Sobień, 2012).

The Uddvide-1 drill core (63.555556°N, 16.890278°E), and nearby outcrop samples, from the island of Gotland, Sweden, are predominantly composed of carbonates from the shallow shelf of the western margin of the Baltic Basin (Younes et al., 2017). Approximately 30 m of the Uddvide-1 drill core, in the Lau CIE interval, consists of a coarsening-upward siliciclastic sequence that is linked to the progradation of a delta into the basin (Eriksson and Calner, 2008). Conodont biostratigraphy is based on nearby sections from southern Gotland within a few kilometers of the sampled drill core (e.g., Jeppsson, 2005). The Lau conodont extinction is defined based on a series of stepwise extinctions beginning with the practical last appearance datum (pLAD) of *Polygnathoides siluricus* (Jeppsson, 2005).

The Priekule-20 drill core (56.443377°N, 21.614994°E) from southwestern Latvia consists of grey shales and marls from a deep-shelf setting near the center of the Baltic Basin. Graptolite biostratigraphy of the Priekule-20 core was constructed using graptolite occurrence data (e.g., Kaljo et al., 1997; Kiipli et al., 2010). The Kozlowskii graptolite extinction event is defined by the LAD of *Neocucullograptus kozlowskii* (Urbanek, 2003; Manda et al., 2012). Neither locality contains both conodonts and graptolites, thus the correlation between them is based on carbon isotope stratigraphy and the combined conodont and graptolite biostratigraphic framework from other Ludfordian sections with interbedded shale and carbonates (Kaljo and Martma, 2006; Lehnert et al., 2007; Manda et al., 2012; Bowman et al., 2019; Fryda et al., 2021).

3. Materials and methods

3.1. Sample preparation

Samples were collected from the Priekule-20 drill core, Latvia, every 2 to 4 m with finer sampling resolution (every 0.5 to 1 m) during the Lau CIE interval (e.g., Kaljo et al., 1997). Samples were collected every 0.5 to 1 m from the Uddvide-1 drill core, Gotland, Sweden, and every 3 m for outcrop samples stratigraphically above the drill core (e.g., Eriksson and Calner, 2008). Intervals with notable diagenetic alteration (recrystallization, pyritization, or iron oxide staining) were avoided while sampling. The outer margins of drill core samples and the weathered edges of outcrop samples were mechanically removed using a water-based, diamond-blade saw. Samples were powdered using either an agate mortar and pestle or an alumina ceramic SPEX8510 ShatterBox. Prior to crushing, approximately 1 g of powder was micro-drilled from carbonate samples for carbonate carbon isotope and I/Ca analyses, all other data are from powdered bulk rock. For detailed methods of previously

Table 1
Summary of local redox proxy background information and additional references. (Algeo and Tribovillard, 2009; Amos et al., 2014; Bagnato et al., 2017; Berner, 1970; Canfield and Berner, 1987; Lyons and Severmann, 2006; Miller et al., 2011; Poulton and Canfield, 2011; Shen et al., 2019; W. Lu et al., 2019)

Proxy	Oxidized Species	Reduced Species	Marine Redox Zone(s)*	Pertinent Lithology	Geographic Scale	Threshold Value(s)	Reference for Threshold Value(s)	Additional References
I/Ca	IO^{3-}	I^{-}	oxygen - nitrate reduction	carbonates	local	0-2.6 µmol/mol anoxic - suboxic >2.6 µmol/mol well-oxygenated	Z. Lu et al., 2016	Z. Lu et al., 2010; W. Lu et al., 2017, 2018, 2019; Hardisty et al., 2014, 2017, 2021
Fe_T/Al	Fe^{3+}	Fe^{2+}	iron reduction	organic-rich shales and mudstones	local	>0.64** anoxic, shuttling of reactive Fe	Raiswell et al., 2008	Berner, 1970; Canfield & Berner, 1987; Canfield et al., 1992, 1996; Poulton & Canfield, 2005, 2011; Lyons & Severmann, 2006; Hardisty et al., 2018; Raiswell et al., 2018
Fe_{HR}/Fe_T			iron - sulfate reduction			<0.38 oxic-suboxic >0.38 anoxic	Raiswell & Canfield, 1998	
Fe_{pyr}/Fe_{HR}						<0.7 ferruginous >0.7 euxinic	März et al., 2008	
[Mn]	Mn^{3+} Mn^{4+}	Mn^{2+}	nitrate (& manganese) reduction			<850 ppm† likely suboxic - anoxic	Morford & Emerson, 1999	Force & Cannon, 1988; Force & Maynard, 1991; Calvert & Pederson, 1993; Algeo & Maynard, 2004; Turgeon & Brumsack, 2006; Boyer et al., 2011
[V]	V^{5+}	V^{4+} V^{3+}	nitrate - iron reduction		local/global	>97 ppm†† suboxic - anoxic	Rudnick & Gao, 2003	Morford & Emerson, 1999; Tribovillard et al., 2006
[Hg] ‡	Hg^{2+}	Hg^{0}	possibly nitrate - iron reduction?			50 ppb†† >62.4 ppb‡‡ likely reducing	Rudnick & Gao, 2014 Grasby et al., 2019	Bower et al., 2008; Sanei et al., 2012; Amos et al., 2014; Bagnato et al., 2017; Shen et al., 2019; Them et al., 2019
[U]	U^{6+}	U^{4+}	iron reduction			>2.8 ppm†† anoxic - euxinic	McLennan, 2001	Morford et al., 2001; Algeo & Maynard, 2004; Tribovillard et al., 2006; Lau et al., 2019
[Mo]	Mo^{6+}	Mo^{5+} Mo^{4+} Mo^{3+} Mo^{2+}	sulfate reduction			>1.5 ppm†† anoxic - euxinic	McLennan, 2001	Algeo & Lyons, 2006; Algeo & Tribovillard, 2009; Miller et al., 2011; Scott & Lyons, 2012; Hardisty et al., 2018

* Based on marine redox ladder as presented in Froelich et al., 1979; Rue et al., 1997; Owens, 2019
** Based on the average lithogenic values of Paleozoic oxic marine shales of 0.53 ± 0.11.
† Average concentration of Mn in modern marine oxic sediments.
†† Upper continental crust values.
‡ Note that Hg is also used as a proxy for volcanism (see Grasby et al., 2019 for review).
‡‡ Average Hg concentration in sedimentary rocks (mostly shales).

Fig. 1. Paleogeographic reconstruction of the late Silurian Baltic Basin region with locations of the Gotland, Sweden, Uddvide-1 drill core and nearby surficial outcrops, and the Latvian Priekule-20 drill core marked by yellow stars (see Bowman et al., 2019 for detailed discussion of correlation and biostratigraphy of the two localities). (For interpretation of the references to color in this figure legend, the reader is referred to the web version of this article.)

published organic carbon isotope, carbonate-associated sulfate and pyrite sulfur isotope data, see Bowman et al. (2019).

3.2. Iodine to calcium ratios

I/(Ca + Mg) ratios were measured at the National High Magnetic Field Laboratory (NHMFL) at Florida State University using an Agilent 7500cs quadrupole inductively coupled plasma mass spectrometer (ICP-MS) according to standard methods (Z. Lu et al., 2010; W. Lu et al., 2017; Hardisty et al., 2014, 2017; Zhou et al., 2014, 2015). Approximately 2–5 mg of carbonate powder was preferentially micro-drilled from the carbonate mud matrix. The carbonate powder was dissolved in 3% HNO_3. Samples were vortexed and centrifuged, and the supernatant was then diluted using 2% HNO_3 to a ~ 50 ppm Ca + Mg solution. Previously samples have been diluted in a matrix of 0.5% HNO_3 and 0.5% tetramethyl ammonium hydroxide; based on replicate sample analyses using this matrix and a matrix of 2% HNO_3, there is no notable difference in I/Ca values between the two methods (Bowman et al., 2020) provided that the samples are analyzed within the day of dissolution. Calibration standards were made fresh each day by serial dilution of a 10 ppm iodine ICP-MS standard from High Purity Standards and with a similar matrix of ~50 ppm Ca + Mg. The long-term accuracy of this procedure ±0.5 μmol/mol is based on replicate measurements of known reference materials (KL1–2, KL1–4; e.g., Hardisty et al., 2014). In deep time, I/Ca values are commonly reported as I/(Ca + Mg), as they are herein, to account for variable carbonate chemistry and the dolomitization of ancient carbonates. For brevity, though, I/(Ca + Mg) will be referred to as I/Ca throughout the paper.

3.3. Carbonate carbon isotope analyses

For the analysis of carbonate carbon isotopes, 0.2–1 mg of carbonate powder, preferentially micro-drilled from micritic matrix where possible, was weighed and acidified with 100% H_3PO_4 at 25 °C for 24 h. The stable carbon and oxygen isotopes of the evolved gas were analyzed using a ThermoFinnigan Delta Plus XP isotope-ratio mass spectrometer (IRMS) at the NHMFL. All carbon and oxygen isotope values are reported in standard delta notation (δ) with units of per mil (‰) relative to the Vienna Pee Dee Belemnite (V-PDB) standard. Based on long-term, replicate analysis of NBS-19 and other lab standards, the analytical precision of $\delta^{13}C_{carb}$ is ±0.05‰ (1σ).

3.4. Sequential iron extraction

Reactive iron species were sequentially extracted from approximately 100 mg of powdered sample using the method outlined by Poulton and Canfield (2005). First, powdered samples were soaked and continuously shaken in a 1 M sodium acetate ($C_2H_3NaO_2$) solution buffered to pH 4.5 for 24 h to extract Fe associated with carbonate phases (Fe_{carb}) including siderite and ankerite. Then for 2 h a 0.29 M sodium dithionite ($Na_2S_2O_4$) solution buffered with 0.35 M acetic acid and 0.2 M sodium citrate to pH 4.8, under continuous shaking, was used to extract Fe associated with oxide phases (Fe_{ox}) including goethite and hematite. Last, samples were soaked in a solution of 0.2 M ammonium oxalate ($C_2H_8N_2O_4{\cdot}H_2O$) and 0.17 M oxalic acid ($H_2C_2O_4{\cdot}2H_2O$) buffered to pH 3.2 with ammonium hydroxide (NH_4OH) for 6 h under continuous shaking to extract Fe in magnetite (Fe_{mag}). After each extraction step, samples were centrifuged and supernatant saved for geochemical analysis. Subsequently, centrifuged samples were rinsed and agitated with ultrapure water, centrifuged again, and decanted before progressing to the next iron extraction step. Supernatant from each extraction step was diluted using 2% ultrapure HNO_3 and analyzed at the NHMFL on an Agilent 7500cs ICP-MS for Fe concentrations. The fraction of Fe in pyrite (Fe_{pyr}) was determined gravimetrically based on a chromium reducible sulfides extraction (Canfield et al., 1986). Highly reactive Fe (Fe_{HR}) was calculated based on the sum of Fe_{carb}, Fe_{ox}, Fe_{mag}, and Fe_{pyr}.

3.5. Elemental concentrations

Bulk elemental compositions were determined through multi-acid digestion. Sample masses of 50 to 100 mg were weighed into teflon beakers and digested in a CEM MARS 6 microwave digestion system to remove organic carbon without volatilizing redox-sensitive trace elements. Samples were completely digested with a multi-acid digestion using various combinations of trace-metal grade HNO_3, HCl, and HF. Acid was added to samples that were kept on heat (120 to 180 °C) for 24–48 h, and dried before adding more acid. Organic matter that remained post-microwaving was oxidized with ultra-pure H_2O_2. After samples were dissolved completely, they were dried and dissolved in 2% HNO_3 for analysis on an Agilent 7500cs ICP-MS at the NHMFL. Blank concentrations were below detection limits and replicate analyses of USGS standard SDO-1 were within 4% of the reported values for Mn, V, U, and Mo.

3.6. Mercury concentrations

Samples were analyzed for Hg at the Geochemistry of Ancient and Modern Environmental Systems (GAMES) Laboratory at the College of Charleston. Approximately 40–80 mg of powder was measured in a Milestone DMA-80 evo rapid mercury analyzer (Shelton, CT). Samples were heated in stages up to 750 °C to volatilize Hg. Volatilized Hg was then collected via gold amalgamation before analysis through atomic

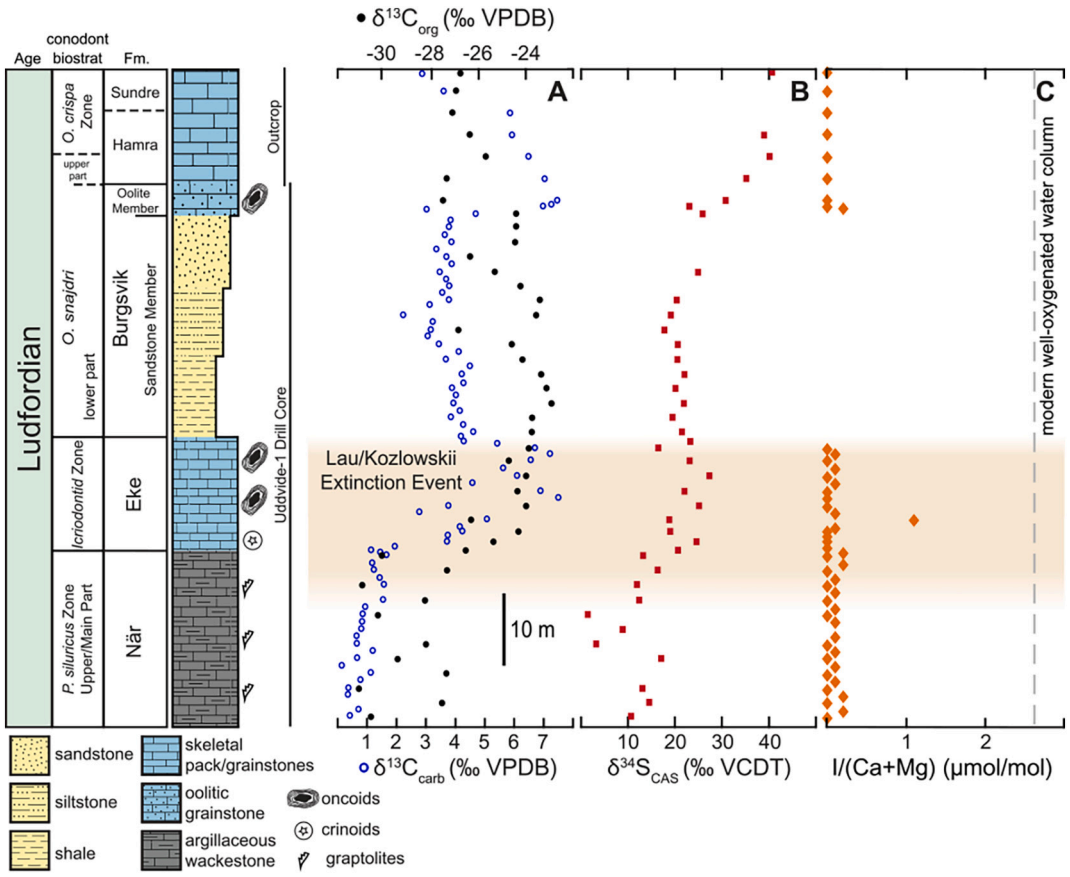

Fig. 2. Stratigraphic column and geochemical data from the Uddvide-1 drill core and related outcrop samples (modified from Bowman et al., 2019). A) Carbonate and organic carbon isotopes. B) Carbonate-associated-sulfate (CAS) sulfur isotopes. C) I/(Ca + Mg) ratios. The Lau/Kozlowskii extinction is highlighted in light orange. Conodont biostratigraphy – *P.: Polygnathoides, O.: Ozarkodina.*

absorption. A liquid standard (serial dilution of ICP-MS standard) was used to calibrate the DMA-80 and two international standards (TORT-3, DORM-4) were used to correct the raw data. All samples contained quantifiable Hg contents. The 2-σ standard deviations of TORT-3 and DORM-4 were 9.4 ng/g ($n = 8$) and 6.6 ng/g ($n = 6$), respectively, which are better than their reported errors. Average 2-σ reproducibility of samples (~22% of total) was ±3.4 ng/g (2-σ range of 0.1 to 4.1 ng/g).

4. Results

The Lau CIE has been previously documented from the Uddvide-1 core, recovered from the island of Gotland, Sweden, as a ~ +7‰ excursion in both $\delta^{13}C_{carb}$ and $\delta^{13}C_{org}$ (Fig. 2A; Younes et al., 2017; Bowman et al., 2019). The Gotland stratigraphic record ends during the falling limb of the Lau CIE, not capturing the return to baseline values. Iodine-to-calcium ratios from the inner shelf carbonates on Gotland are low throughout the sampled interval (Fig. 2C). Most values before and during the CIE range from 0 to 0.2 μmol/mol – at or below the detection limit of this analysis. In the middle of the Eke Formation, during the rising limb of the CIE, there was a single higher value at 1.1 μmol/mol. The siliciclastic interval in the Uddvide-1 core, the Burgsvik Sandstone Member, was not analyzed for I/Ca ratios.

Additional carbon isotope data from the deep shelf mudstones, the Priekule-20 core, Latvia, record the highest peak values of the Lau carbon isotope excursion at this locality as +5.8‰ in the Nova Beds of the Dubysa Formation (Fig. 3A). Total organic carbon was relatively high, but variable, at values between 0.6 and 1.2% in the Šešupe Member of the Dubysa Formation (Fig. 3B). Total organic carbon then decreases notably through the Nova Beds to ~0.2% by the peak of the CIE and stayed low through Engure and Mituva formations. Pyrite-sulfur abundances follow a similar trend, with higher, but variable, values between 0.3 and 0.9% pre-CIE, which then decrease through the Nova Beds to values between 0 and 0.2% from the falling limb of the CIE into the post-excursion baseline (Fig. 3D). As with the offset between the peaks of the carbon and sulfur isotope excursions (Fig. 3A, C) noted by Bowman et al. (2019), pyrite-sulfur content has a slower decline than that of TOC.

The Fe_{HR}/Fe_T values ranged from 0.05–0.35 throughout the Priekule-20 core, averaging 0.16 with no notable trends in the data (Fig. 4A). The ratios of Fe_{pyr}/Fe_{HR} were high through the Šešupe Member and ranged between 0.61 and 0.94 (Fig. 4B). Fe_{pyr}/Fe_{HR} values dropped through the Nova Beds and lower Engure Formation, in concert with the decrease in pyrite-sulfur content, to values of 0.03–0.48 through the upper Engure and Mituva formations. The Fe_T to Al ratios were nearly constant throughout the sampled interval of the core, ranging from 0.40–0.54, averaging 0.47 (Fig. 4C). Manganese concentrations, as reported by Bowman et al. (2019), are low throughout the section. Concentrations ranged between 308 and 596 ppm, with lower average values (~381 ppm) through the Dubysa Member and slightly higher average values (~532 ppm) from the Nova Beds through the Mituva Formation (Fig. 4D). Through the Šešupe Member, V concentrations were high, with values averaging ~119 ppm before coming to a peak of 188 ppm just below the Nova Beds at the start of the rising limb of the CIE (Fig. 4E). The V concentrations then dropped to an average of ~68 ppm through the CIE and the post-excursion baseline (the Nova Beds to the Mituva Formation). Concentrations of Hg followed a nearly identical stratigraphic trend through the section, with higher average values of ~78 ng/g, which rose to a peak of ~110–120 ng/g before falling to lower average values of ~24 ng/g (Fig. 4F). The U and Mo concentrations had similar stratigraphic trends to V and Hg, with higher

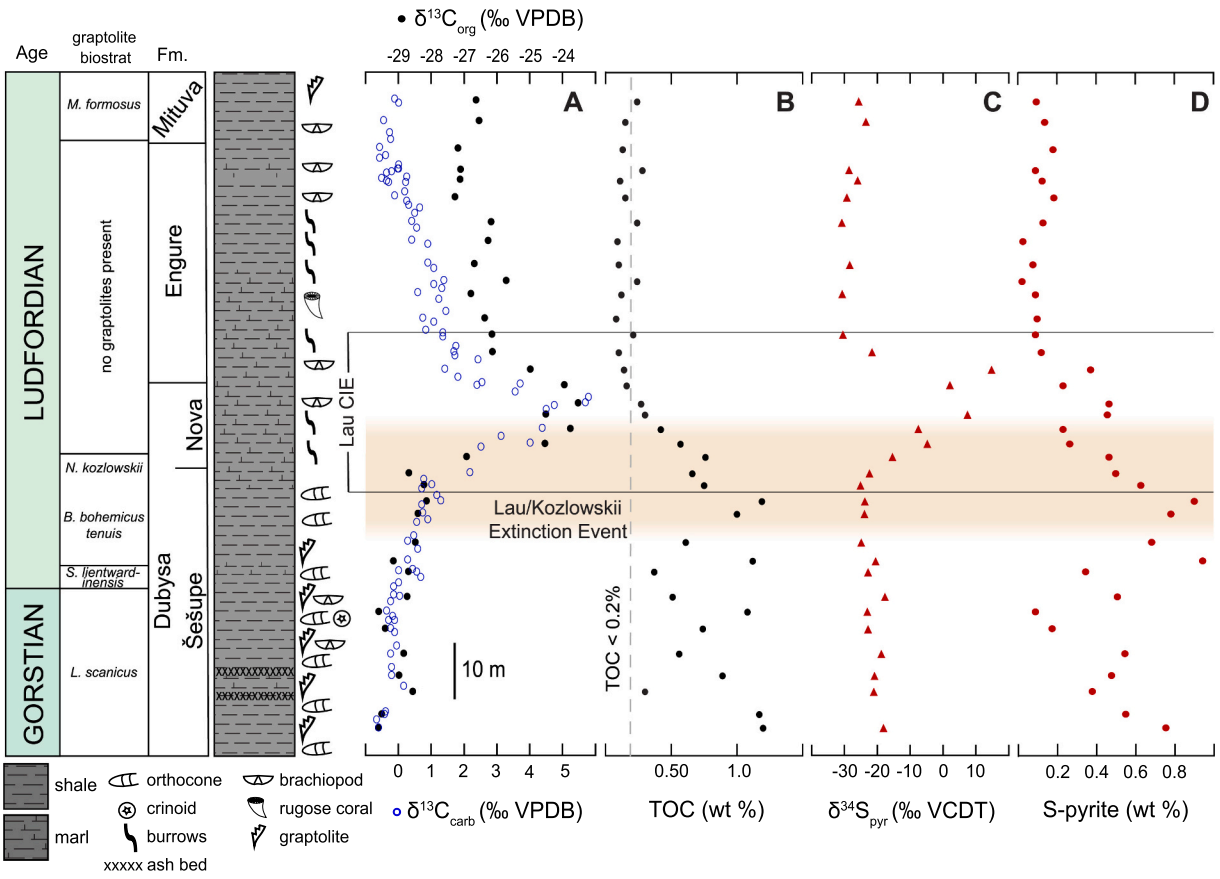

Fig. 3. Stratigraphic column for the Priekule-20 drill core with carbon and sulfur geochemical data (modified from Bowman et al., 2019). A) Carbonate (carb) and organic (org) carbon isotope data. B) Total organic carbon (TOC) weight percent. C) Pyrite (pyr) sulfur isotope data. D) Pyrite sulfur weight percent. The Lau CIE interval is outlined in thin black lines, the Lau/Kozlowskii extinction event is highlighted in light orange; wt%: weight percent. Graptolite biostratigraphy – *L.: Lobograptus, S.: Saetograptus, B.: Bohemograptus, N.: Neocucullograptus, M.: Monograptus.*

average values low in the section and lower average values in the upper part of the section, but with even more notable peaks in the upper Šešupe Member. The U concentrations in the lower part of the section averaged ~4.4 ppm, then rose to a peak of 8.9 ppm in the early LKE interval, and then decreased to an average of ~2.1 ppm by the late LKE interval and throughout the upper part of the section (Fig. 4G). The Mo concentrations averaged ~3.3 ppm in the lower part of the studied core, then rose to a peak of 24 ppm in the early LKE interval, and subsequently declined to an average of 0.3 ppm by the late LKE interval throughout the remainder of the study interval (Fig. 4H). All trace metal concentrations are reported as absolute concentrations, carbonate-corrected concentrations, and TOC-normalized concentrations. The carbonate-corrected concentrations are used to account for variable carbonate content in the Latvian Priekule-20 core (Fig. 4D-H). Carbonate content averages 31.5% in the Priekule-20 core, but there is significant variability, with a standard deviation of ±15.3%. The carbonate-correction, however, does not significantly impact any of the stratigraphic trends that are present in the absolute trace metal data. The TOC-normalized concentration data have similar trends to the absolute concentrations in the lower part of the core (upper Gorstian and lower Ludfordian). Trends in V/TOC, Hg/TOC, and U/TOC diverge from the absolue concentrations in the middle and upper Ludfordian with notably higher values in the TOC-normalized data in the upper part of the core.

5. Discussion

5.1. Local redox conditions of the shallow shelf

The Gotland shallow shelf carbonate setting has been previously examined for diagenetic influence, and there has been little evidence found for meteoric diagenesis or thermal alteration (Eriksson and Calner, 2008; Bowman et al., 2019). Cross-plotted carbonate carbon and oxygen isotope data show no significant correlation to indicate the effects of meteoric diagenesis (Bowman et al., 2019). Moreover, conodont studies of the Ludfordian strata of Gotland report very low conodont color alteration index (CAI) values of ≤1, making thermal alteration unlikely (Jeppsson, 1983).

Most I/Ca values before and after the CIE ranged from 0 to 0.2 μmol/mol with a single higher value at 1.1 μmol/mol during the rising limb of the CIE (Fig. 2C). While the calcitic cements of the Burgsvik Sandstone were not analyzed for I/Ca, the shallower-water deposition of the clastic, prograding delta facies during the interval of lowest sea level in the Ludfordian (i.e., deposition within the well-oxygenated mixed layer) makes it likely that I/Ca values would have been higher at that time (Eriksson and Calner, 2008). Modern, well-oxygenated water columns typically have I/Ca ratios of 2.6 μmol/mol or higher (Z. Lu et al., 2016). As water column oxygen concentrations decrease though, iodate is rapidly reduced to iodide, and the primary electron acceptor used by microbial metabolisms begins to shift from oxygen to nitrate or lower based on the marine redox ladder (e.g., Rue et al., 1997). Near-zero values for I/Ca are interpreted as either carbonate precipitation/deposition under anoxic conditions with quantitative, or near-quantitative, reduction of IO_3^- to I^- (Z. Lu et al., 2010), or as having been diagenetically reset by the flow of reducing fluids (Hardisty et al., 2017). There is little evidence to suggest that this section experienced significant post-burial diagenetic alteration that could have lowered I/Ca values (Bowman et al., 2019). Thus, while diagenetic resetting of the I/Ca values is possible, the consistently low values suggest that the

sampled interval of the lower to middle Ludfordian of the Gotland shallow shelf carbonate succession was likely deposited in or near an adjacent OMZ (Z. Lu et al., 2010; W. Lu et al., 2018; Owens et al., 2017; Bowman et al., 2020; Hardisty et al., 2021). There were no significant changes in local redox conditions before or during the Lau CIE along the shallow shelf of the Baltic Basin. This was likely because the carbonate succession records primarily the lower and middle Ludfordian (Fig. 6A, B), which represent the interval of time that was most reducing both locally and globally as bottom-water deoxygenation initiated and expanded (Tl excursion: Bowman et al., 2019; U isotopes: del Rey et al., 2020) and later the burial of organic carbon and pyrite increased (CIE, sulfur isotope excursion: Bowman et al., 2019, 2020).

5.2. Local redox conditions of the deep shelf

The possibility of diagenetic alteration of the shales and marls of the Latvian deep shelf setting has also already been explored by Bowman et al. (2019). Cross-plotted TOC and $\delta^{13}C_{org}$ data indicate the possibility for some amount of thermal alteration, likely due to burial as the Silurian strata of Latvia are relatively flat-lying. Low conodont CAI values from other drill cores in the same area of Latvia, however, suggest thermal heating was limited (CAI = 1; Kaljo et al., 1997; Nehring-Lefeld et al., 1997). Sedimentation rates (undecompressed) for this part of the Baltic Basin deep shelf are estimated to be between 6.46 and 8.18 cm/ky through the Ludfordian (see Bowman et al., 2019 for sedimentation rate calculations) – and were even higher in the foredeep of the Caledonian orogen to the southeast at ~10.75 cm/ky (Kozłowski and Sobień, 2012). Based on the sedimentation rate data compiled in Sadler (1981), these rates are approximately an order of magnitude higher than estimates from sections of terrigenous shelf/slope environments of similar stratigraphic extent and time span. Sedimentation rates have the potential to mask changes in redox proxies, particularly the accumulation of redox-sensitive major and trace elements through authigenic processes under reducing conditions (Lyons and Kashgarian, 2005; Hardisty et al., 2018), such as with the shuttling of reactive iron within a basin or the reduction of uranium at the sediment-water interface.

Local redox conditions are assessed herein based, first, upon the speciation of iron into different mineral components (Fig. 4A-C). While high sedimentation rates are likely masking the signature of locally reducing conditions in the iron speciation data from the deep shelf of the Baltic Basin, we conservatively interpret the trace metal data presented here (Fig. 4D-H, 5) as being largely representative of local rather than global changes in redox conditions. The details of the local redox conditions in the deep shelf of the Baltic Basin are discussed in three parts: the upper Gorstian through the lower Ludfordian (the Šešupe Member of the Dubysa Formation; from the *Lobograptus scanicus* biozone to the lower *Bohemicus bohemicus tenuis/N. kozlowskii* biozone), the lower–middle Ludfordian (uppermost Šešupe Member of the Dubysa Formation; the upper *N. kozlowskii* biozone), and the middle–upper Ludfordian (the Nova Beds of the Dubysa Formation and the Engure and Mituva Formations, from just above the *N. kozlowskii* biozone to the *Monograptus formosus* biozone). The trace metal data are discussed in order of decreasing redox potential and, generally, absolute concentration data are referenced as neither carbonate nor aluminum normalization significantly changed the stratigraphic trends. TOC-normalized trace metal data are also discussed, particularly for the middle to upper Ludfordian, as the trends vary notably from that of the absolute concentration data for V, Hg, and U.

5.2.1. Upper Gorstian to lower Ludfordian: Within an OMZ

Values of Fe_{HR}/Fe_T ranged between 0.05 and 0.35 in the oxic to possibly anoxic fields (Raiswell and Canfield, 1998) throughout the entire sampled interval from the upper Gorstian to the lower Ludfordian and on through the upper Ludfordian (Fig. 4A). This could indicate that the water column was consistently oxygenated (or not reaching Fe reduction), that redox conditions were variable, or that sedimentation

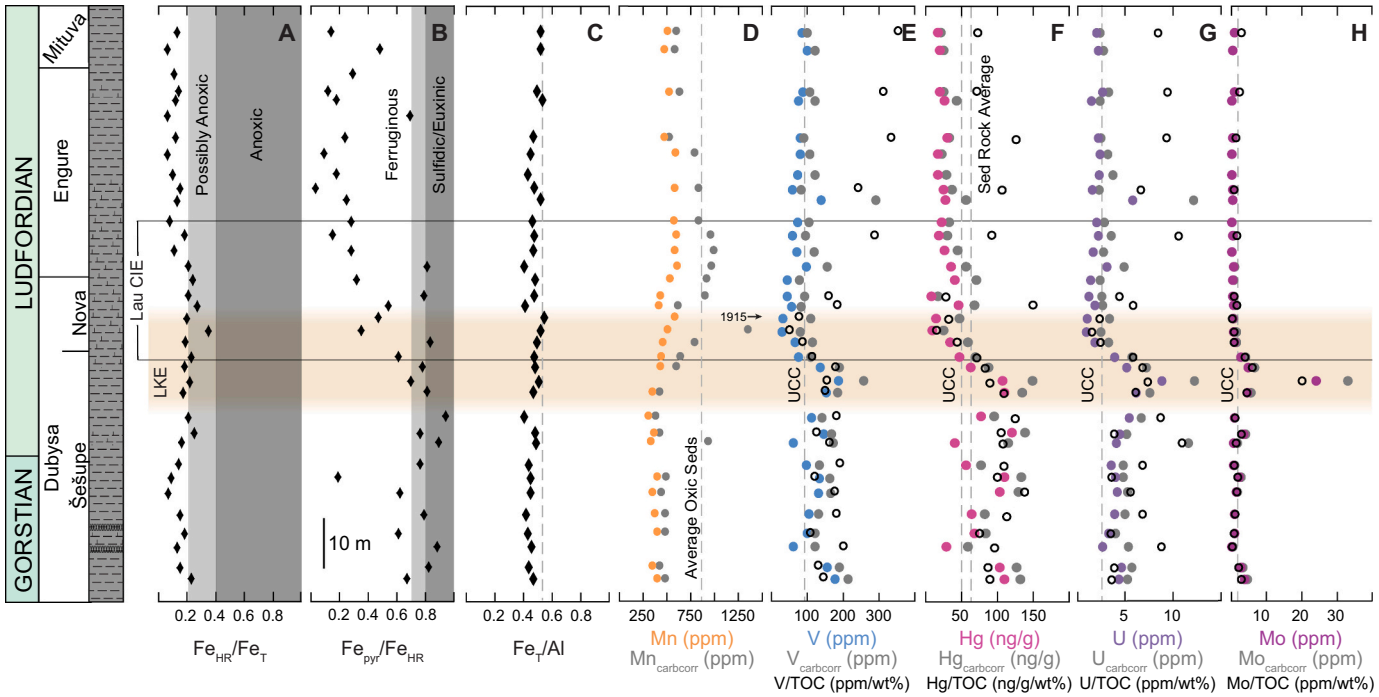

Fig. 4. Iron speciation and trace metal data from the Priekule-20 drill core. A) Highly reactive (HR) to total (T) iron (Fe) ratios. B) Pyrite (pyr) to highly reactive iron ratios. C) Total iron to aluminum ratios. D) Absolute and carbonate-corrected manganese (Mn) concentrations. *E*-H) Absolute, carbonate-corrected, and TOC-normalized vanadium (V), mercury (Hg), uranium (U), and molybdenum (Mo) concentrations. The Lau CIE interval is outlined in thin black lines, the Lau/Kozlowskii extinction is highlighted in light orange; carbcorr: carbonate-corrected, UCC: upper continental crust.

rates were high enough to dilute or prevent the accumulation of highly reactive iron species (Hardisty et al., 2018; Raiswell et al., 2018). Fe_{pyr}/Fe_{HR} values were high through the upper Gorstian and lower Ludfordian strata, typically above the euxinic threshold of 0.70, with most highly reactive iron minerals forming pyrite after the production of hydrogen sulfide as a by-product of microbial sulfate reduction (Fig. 4B). Combined with the low Fe_{HR}/Fe_T, the high Fe_{pyr}/Fe_{HR} values suggest high concentrations of sulfide present (i.e., in the sulfate reduction zone) in sediment porewaters rather than the water column, as is observed at the modern Long Island Sound FOAM site (Raiswell and Canfield, 1998; Hardisty et al., 2018). As with Fe_{HR}/Fe_T, the Fe_T/Al values were relatively constant throughout the entire sampled interval, averaging 0.47, just below the average lithogenic value of Paleozoic oxic marine shales (Fig. 4C; e.g., Raiswell et al., 2008). This is indicative of a lack of benthic iron shuttling from the shallow portions of the basin to the deeper shelf sediments (Canfield et al., 1996; Raiswell and Canfield, 1998; Hardisty et al., 2018; Raiswell et al., 2018). This could also be an artifact of high sedimentation rates or could suggest that the iron reduction zone of the marine redox ladder was only within the sediment porewaters rather than the lower water column. Manganese (Mn) concentrations were low through the Gorstian and lower Ludfordian, averaging 381 ppm, well below the average oxic sediment concentration of 850 ppm (Fig. 4D; Calvert and Pederson, 1993; Morford and Emerson, 1999; Turgeon and Brumsack, 2006; Boyer et al., 2011). This suggests that bottom waters were suboxic to anoxic, resulting in the reductive dissolution of Mn-oxides and preventing their further precipitation and burial (Force and Cannon, 1988; Force and Maynard, 1991; Dickens and Owen, 1994; Algeo and Maynard, 2004; Owens et al., 2017).

Vanadium (V) concentrations averaged 119 ppm through the Gorstian and lower Ludfordian, modestly enriched in comparison to UCC values of 97 ppm (Fig. 4E; Rudnick and Gao, 2003). In extremely reducing environments, such as those with euxinic conditions, V can be enriched to concentrations of hundreds to thousands of ppm (e.g., Owens et al., 2016, 2017; Young et al., 2020). The minor to moderate enrichment in the Baltic Basin was likely representative of locally suboxic to anoxic conditions in the deep shelf water column, possibly through either the nitrate or iron reduction zones of the marine redox ladder (Tribovillard et al., 2006; Canfield and Thamdrup, 2009). Mercury (Hg) was also enriched in this interval (Fig. 4F) and had an overall trend very similar to those of V and U. Average Hg concentrations in the upper Gorstian and lower Ludfordian were ~ 78 ng/g, which is slightly above the average concentrations of both sedimentary rocks, at 62.4 ng/g, and upper continental crust, at 50 ng/g (Rudnick and Gao, 2014). To inform our interpretation of the Hg concentration data, we normalized the raw concentration data to TOC (Figs. 4F, 5C), pyrite-sulfur (Fig. 5D), and aluminum (Fig. 5E), to account for the most likely host mineral phases of Hg (e.g., Grasby et al., 2019; Shen et al., 2020). The trend in Hg/Al was almost identical to that of the absolute Hg data, as Al concentrations were fairly static through the sampled strata aside from short intervals where carbonate content was particularly high (see Supplemental Data file). This suggests that the enrichment in Hg in the Gorstian to lower Ludfordian was not the result of Hg adsorption onto clay minerals or changes in the input of terrigenous material (Sanei et al., 2012). The challenge in the interpretation of Hg concentrations is assessing whether enrichments in Hg are due to increased loading from variations in atmospheric deposition (i.e., fluctuations in volcanic outgassing) or increased sequestration from changes in local OM flux and/or redox conditions (Bower et al., 2008; Sanei et al., 2012; Grasby et al., 2019; Them II et al., 2019). Trends in normalized Hg/TOC (Fig. 5C) and Hg/S-pyrite (Fig. 5D) data during the upper Gorstian and lower Ludfordian largely reflect those of the absolute concentrations but are notably enriched above absolute concentrations in the upper Ludfordian (see Section 5.2.3). There were outliers in each of the datasets that could be misinterpreted as excursions in either set of normalized data. In all

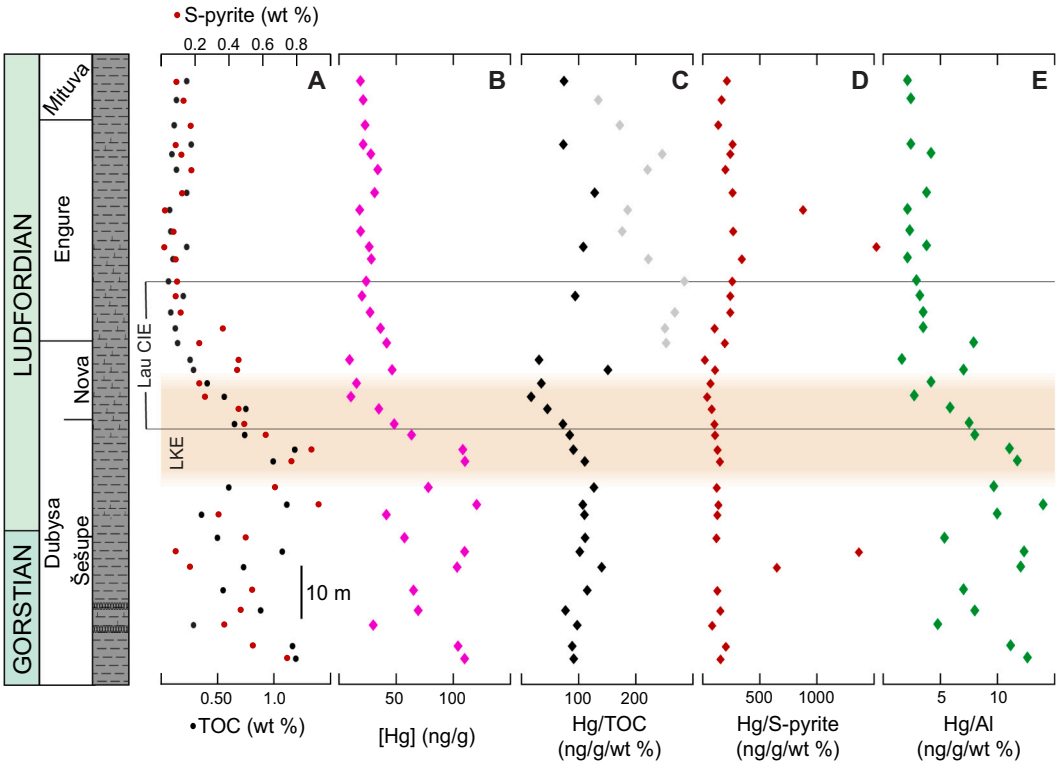

Fig. 5. Normalized mercury and related geochemical data from the Priekule-20 drill core. A) Total organic carbon and pyrite sulfur concentrations. B) Mercury (Hg) concentrations. C) Mercury normalized to total organic carbon (TOC), grey diamonds represent Hg/TOC data from samples where TOC content is below the analytical precision of the method (i.e., <0.2%). D) Mercury normalized to pyrite-sulfur concentrations. E) Mercury normalized to aluminum (Al) concentrations. The Lau CIE interval is outlined in thin black lines, the Lau/Kozlowskii extinction is highlighted in light orange.

cases, however, the outliers observed had either low TOC wt% (at the lower limits for analytical precision,< ~0.2%) or pyrite concentrations were near zero. Additionally, there are no known emplacements of large igneous provinces in the late Silurian. The only K-bentonite ash beds in the studied portion of the Priekule-20 core are from the upper Gorstian interval, which has no associated Hg/TOC anomaly, making increased loading of Hg to the environment an unlikely explanation for the trends in the data. Last, this study site was located in a distal location within the Baltic Basin, and previous work has suggested that depositional settings simililar to this may not be ideal for recording changes in atmospheric Hg cycling (e.g., Them II et al., 2019). Altogether, these indicate that the Hg enrichments in the Gorstian and lower Ludfordian were caused by redox- and preservation-related mechanisms. This is further supported by the strong correlations between Hg and TOC, along with Hg and S-pyrite, with R^2 values of 0.78 and 0.77, respectively.

Uranium (U) concentration data show only minor enrichments through the Gorstian and lower Ludfordian, with average concentrations of 4.4 ppm in comparison to the UCC value of 2.8 ppm (Fig. 4G; McLennan, 2001). In modern anoxic marine settings, the enrichment of U occurs near the sediment-water interface or within sediment pore spaces, rather than in the water column; thus U concentrations are interpreted to be a proxy for bottom-water anoxia (Lau et al., 2019). The minor enrichments in U observed in the Baltic Basin are likely due to suboxic to anoxic bottom waters. Molybdenum (Mo) also only has minor enrichments through this time interval, with average concentrations of 3.3 ppm compared to UCC values of 1.5 ppm (Fig. 4H; McLennan, 2001). When Fe_{pyr}/Fe_{HR} values are high, as they are in the Gorstian and lower Ludfordian strata from Latvia, low enrichments of Mo from 2 to 25 ppm are interpreted to have been associated with sulfidic porewater conditions beneath oxic to anoxic water column conditions (e.g., Scott and Lyons, 2012; Hardisty et al., 2018).

Based on trace metal cycling research focused on reducing marine environments within modern OMZs (Scholz, 2018 and references therein) and the paleo-redox conventions proposed by Canfield and Thamdrup (2009), the Gorstian and lower Ludfordian strata in this area were likely deposited within a nitrogenous OMZ. Water column redox conditions would have been reducing enough that oxygen was no longer the primary electron acceptor but not reducing enough for the extensive cycling of iron (Fig. 6A). Many modern OMZs with similar geochemical signatures have been termed "nitrogenous" as they have low oxygen concentrations and the respiration of organic matter occurs primarily through nitrate reduction via denitrification (the reduction of nitrate, NO_3^-, to nitrite, NO_2^-, and gaseous nitrogen compounds) and anaerobic ammonia oxidation (NO_2^- reduced to N_2 gas; Gruber and Sarmiento, 1997; Kuypers et al., 2005; Hammersley et al., 2007; Lam and Kuypers, 2011; Scholz, 2018). Manganese concentrations are low in the sediments underlying these modern nitrogenous OMZs, due to the reductive dissolution and bacterial reduction of Mn-oxide minerals, which, like the reduction of iodate, straddles the boundary of the oxygen and nitrate reduction zones on the marine redox ladder (Force and Cannon, 1988; Force and Maynard, 1991; Dickens and Owen, 1994; Turgeon and Brumsack, 2006; Scholz, 2018). Manganese concentrations were low through the Gorstian and lower Ludfordian (Fig. 4D). Vanadium is first reduced and accumulates in sediment under suboxic to anoxic conditions in the nitrate and iron reduction zones of the marine redox ladder and is further enriched under euxinic conditions in the sulfate reduction zone (Morford and Emerson, 1999; Tribovillard et al., 2006). Concentrations of V in the upper Gorstian and lower Ludfordian were moderately enriched above UCC values, averaging ~119 ppm. The moderate enrichment of V supports the idea of deposition under the anoxic conditions of a nitrogenous OMZ along the deep shelf. The similarity in the stratigraphic profiles of V and Hg suggests that Hg can also become enriched under suboxic to anoxic conditions as it is buried with organic matter and/or adsorbed onto sedimentary pyrite in sulfidic porewaters in open connection with the overlying water column. This also suggests that the water column would have likely been in the manganese to

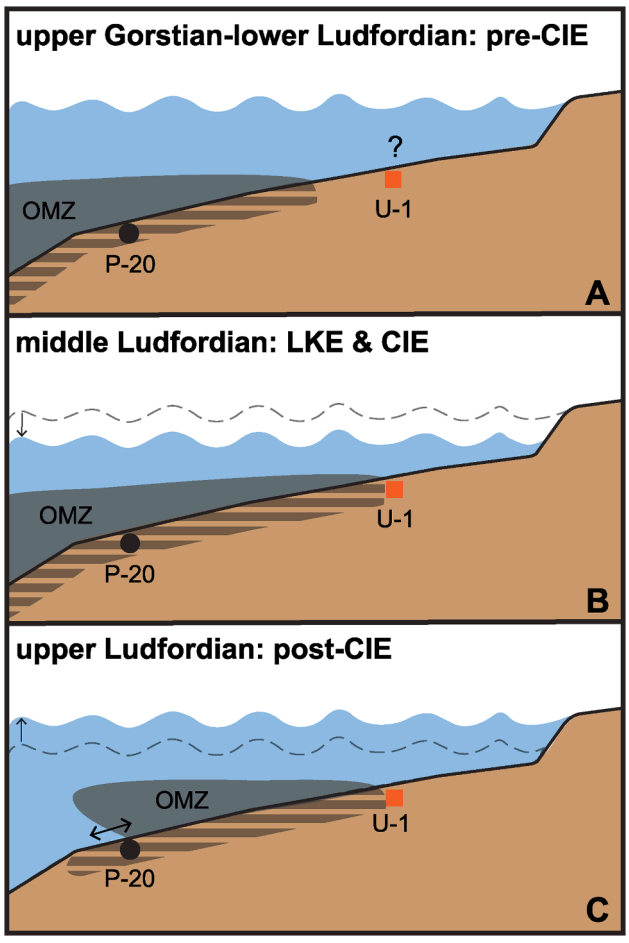

Fig. 6. Schematic paleoceanographic reconstruction of the redox and sea-level changes in the Baltic Basin during the late Silurian (see sections 5.2 and 5.3 for discussion). Relative positions of the study sections are noted, water column reducing conditions are denoted by grey shading, sediment porewater reducing conditions are denoted by grey striped shading. A) Upper Gorstian – lower Ludfordian. B) Middle Ludfordian. C) Upper Ludfordian. U-1: Uddvide-1 core; P-20: Priekule-20 core; OMZ: oxygen minimum zone. Question mark represents temporal uncertainties in local redox conditions.

nitrate reduction zones, with sulfate reduction in the sediment porewaters, as is the case in many modern OMZs (e.g., Scholz et al., 2011, 2016). Based on low Fe_{HR}/Fe_T values, and Fe_T/Al values within one standard deviation of Paleozoic lithogenic values, water column redox conditions were not sufficiently reducing within the OMZ for the cycling of Fe between the sediments and water column (i.e., lack of benthic Fe shuttle). Any Fe cycling was likely happening within sediment porewaters or at the sediment-water interface and would have been diluted by the high sedimentation rates mentioned previously. The low enrichments of U and Mo also fit well with the proposed environmental interpretation of a moderately-reducing, nitrogenous OMZ in the deep shelf of the Baltic Basin at this time. The lack of evidence for benthic Fe shuttling within the lower water column of the nitrogenous OMZ explains the low enrichments of U, which is typically reduced across the sediment-water interface when the iron reduction zone falls along the interface (Morford et al., 2001; Tribovillard et al., 2006; Lau et al., 2019). Molybdenum is most effectively reduced and accumulates in sediments under sulfidic/euxinic conditions in the sulfate reduction zone, under even more reducing conditions on the marine redox ladder (Algeo and Lyons, 2006; Scott and Lyons, 2012). The low to moderate enrichments of trace elements through the upper Gorstian and lower Ludfordian may have been influenced by the high sedimentation rates discussed previously, wherein higher sedimentation rates could be

diluting the accumulation of redox-sensitive trace elements, leading to relatively conservative interpretations of the upper Gorstian and lower Ludfordian local redox conditions. However, the stratigraphic trends observed for the trace elements are not likely to be a product of changing sedimentation rates as normalizing trace element concentrations to aluminum did not impact their trends.

5.2.2. Lower to middle Ludfordian: Sulfidic event within the OMZ

In the stratigraphic trends of the trace metals that become enriched under reducing conditions (i.e., V, Hg, U, Mo), there was a peak in concentrations in the upper Šešupe Member of the Dubysa Formation in the lower-middle Ludfordian (Fig. 4E-H). Additionally, burial of organic matter and pyrite were high (Fig. 3B, D), Fe_{pyr}/Fe_{HR} values were high (Fig. 4B), and Mn concentrations were particularly low (Fig. 4D) during this time interval. We interpret this stratigraphic interval in the upper Šešupe Member to be representative of deposition within a nitrogenous OMZ during the most locally reducing conditions along the deep shelf of the Baltic Basin through the Ludfordian. It is possible that this interval of most locally reducing conditions (i.e., peaks in trace metal abundances in the LKE interval) represents a brief interval of time (possibly ca. 10 ky) when free hydrogen sulfide expanded within the local bottom waters of the primarily nitrogenous OMZ, rather than only being present in the sediment porewaters. Thus the sulfate reduction zone may have migrated into the water column and enhanced the sequestration of trace metals into the underlying sediments. Similar phenomena have been recorded in the modern Peruvian and Namibian OMZs on a seasonal to interannual basis (Brüchert et al., 2003; Schnuck et al., 2013). Notably, this possible transient sulfide event within the OMZ of the Baltic Basin was coincident with the early extinction stages of the LKE event and directly proceeded the onset of the Lau CIE when the amount of organic carbon burial would have increased significantly.

5.2.3. Middle to upper Ludfordian: On the edge of the OMZ

Subsequently in the middle Ludfordian, during the falling limb of the Lau CIE and the coincident sulfur isotope excursion, values of Fe_{pyr}/Fe_{HR} decreased to an average of 0.25 (Fig. 4B), well below the euxinic threshold of 0.70 (Canfield et al., 1992; Raiswell and Canfield, 1998; März et al., 2008), coeval with decreased local pyrite burial (Fig. 3D). Although pyrite burial still occurred at this locality, it was no longer the primary reactive iron species being buried. This suggests that the sulfate reduction zone of the marine redox ladder where pyrite would have been accumulating was likely deeper within local marine sediments. In the upper Ludfordian, Fe_{HR}/Fe_T values were low and Fe_T/Al values were similar to that of average Paleozoic oxic marine shales, as they were in the Gorstian and lower Ludfordian, suggesting minimal to no benthic iron shuttle (Fig. 4A, C). Manganese concentrations were still low, averaging 532 ppm through the middle and upper Ludfordian; higher than the upper Gorstian and lower Ludfordian but still lower than that of average oxic sediments (Fig. 4D; Calvert and Pederson, 1993; Morford and Emerson, 1999; Turgeon and Brumsack, 2006; Boyer et al., 2011). This implies that bottom waters were still suboxic to anoxic, preventing the precipitation of Mn-oxide minerals, but were likely less reducing than earlier in the Ludfordian.

Concentrations of V, Hg, U, and Mo all decreased to lower average concentrations, which were generally lower than UCC values, through the middle to upper Ludfordian strata within the Priekule-20 core. This could have been due solely to changes in local redox conditions (explored here) or could have been the result of an overprint of global changes in redox on the local paleo-redox record (see Section 5.3 below). Concentrations of V were somewhat variable but decreased to an average of 68 ppm, compared to the UCC value of 97 ppm (Fig. 4E; Rudnick and Gao, 2003). This could be the result of suboxic water column conditions or fluctuating redox conditions, possibly with oxygen and nitrate variably acting as the primary electron acceptor of microbial metabolisms in the water column. Similarly, Hg concentrations, while variable, decreased to an average of 24 ng/g in the upper Ludfordian, which is lower than both the UCC value and the sedimentary rock average (Fig. 3F; Rudnick and Gao, 2014). This could also be tied to less reducing conditions locally and, like the previously enriched values, was certainly related to organic matter and pyrite burial, both of which decrease into the upper Ludfordian (Fig. 3B, D; Bower et al., 2008; Sanei et al., 2012; Grasby et al., 2019; Them II et al., 2019). Concentrations of U were also variable but decreased through the same stratigraphic interval to an average of 2.1 ppm, just below the UCC value of 2.8 ppm (McLennan, 2001). Molybdenum concentrations decreased to an average of 0.3 ppm in the upper Ludfordian in comparison to UCC values of 1.5 ppm (McLennan, 2001). The lower average concentrations in both U and Mo suggest that the zones of iron and sulfate reduction were likely even deeper within the sediments of the deep shelf.

Through this change in local paleo-redox conditions, there is no evidence to imply a change in sedimentation rate or terrigenous input. The carbonate-corrected trace metal data also rule out the possibility that the decrease in trace element concentrations could have been the result of dilution due to a change in the type of sedimentation (i.e., higher percentage of carbonate vs. siliciclastic material; grey symbols Fig. 4E-H). TOC-normalized trace metal data, however, are higher than the absolute and carbonate-corrected data in the upper Ludfordian for V, Hg, and U (black symbols Fig. 4E-G). Data where TOC wt% was less than 0.2% (i.e., light grey symbols Fig. 5C) were not included in the trends of TOC-normalized data in Fig. 4 to avoid the appearance of excursions/anomalies in the data resulting from TOC contents determined to be below analytical precision of the method. V/TOC in the upper Ludfordian were as high as 356 ppm/wt%, 3–6 times higher than absolute concentrations (Fig. 4E). Hg/TOC reached concentrations of 125 ng/g/wt%, more than double the coeval absolute Hg concentrations and similar to the Hg/TOC values of the upper Gorstian and lower Ludfordian (Fig. 4F). U/TOC data of the upper Ludfordian were likewise similar to concentrations in the lower part of the core when local water column redox conditions were more clearly reducing, 2–5 times higher than the coincident absolute concentrations (Fig. 4G). Mo/TOC values remain low through the upper Ludfordian. These TOC-normalized trace metal data imply more strongly reducing conditions along the deep shelf in the upper Ludfordian than is suggested by the absolute concentrations.

Based upon these interpretations, and comparison to modern open ocean marine OMZs, we suggest that the middle to upper Ludfordian strata were deposited under suboxic water column conditions just below (i.e., basinward) or along the boundary of the nitrogenous OMZ (Fig. 6C; Scholz, 2018 and references therein). Sediments below modern OMZs often have high Fe_T/Al values as a result of benthic iron shuttling (Scholz et al., 2014). Elevated Fe_T/Al values were not observed in the middle to upper Ludfordian strata here, but this could once again be explained by a lack of benthic iron shuttling in the overlying OMZ or dilution due to high sedimentation rates. A location at or just below the lower boundary of an OMZ would still have had minimal cycling of trace metals through the open connection between the sediment porewaters and the overlying suboxic water column. Furthermore, at the periphery of the nitrogenous OMZ, redox conditions likely would have fluctuated between the oxygen and nitrate reduction zones of the marine redox ladder (Fig. 6C). A combination of these two factors could explain why Mn concentrations remained low and V, Hg, and U had variable concentrations that were all still intermittently enriched above UCC values, with TOC-normalized data consistently higher than absolute concentrations (Scholz, 2018). The accumulation of sulfide, even in sedimentary porewaters, was likely minimal through the upper Ludfordian given the depleted Mo concentrations (absolute and TOC-normalized) and low Fe_{pyr}/Fe_{HR} values.

5.3. Global marine redox implications

The lowest Mn concentrations, peaks in trace metal enrichments, and high Fe_{pyr}/Fe_{HR} in the lower-middle Ludfordian represent the most

locally reducing conditions in the water column of the deep shelf, possibly due to a sulfidic event within the nitrogenous OMZ (Brüchert et al., 2003; Schnuck et al., 2013; Scholz, 2018). Just after this peak in trace metal enrichments, in the middle Ludfordian during the rising limbs of the Lau CIE and the associated sulfur isotope excursion, there was a prominent decrease in the absolute and carbonate-corrected concentrations of V, Hg, U, and Mo until they were depleted below UCC values (Fig. 4E-H).

While we have largely interpreted the trends in trace metal enrichment and depletion recorded in the deep shelf of the Baltic Basin as being representative of local changes in redox conditions, it is possible to draw inferences about global changes in marine redox when considering the data collectively and in the context of other global marine redox proxy work that has been done throughout this interval in the Silurian (i.e., Bowman et al., 2019, 2020; del Rey et al., 2020; Fryda et al., 2021). The significant decrease in trace metal concentrations occurs during the early to middle Ludfordian, when records of Tl, U, and S isotopes suggest the most reducing marine conditions were expanding globally (Bowman et al., 2019, 2020; del Rey et al., 2020). As the fraction of anoxic and euxinic waters expand in the global ocean, trace metals are more readily sequestered into reducing sediments (e.g., Cretaceous OAE2, Owens et al., 2016). Thus, we suggest that the sharp decrease in trace metal concentrations through the lower to middle Ludfordian, which occurs when reducing conditions should be the most prevalent, could be the overprint of a global drawdown of trace metal inventories onto the shift in local paleo-redox conditions. If the decrease in trace metal concentrations was primarily the result of a global trace metal drawdown, it is possible that the middle to upper Ludfordian sediments of the deep shelf may have been deposited under more reducing conditions than that of the boundary of the nitrogenous OMZ. These global interpretations of our trace metal datasets remain speculative as there is not a long-term, open ocean euxinic deposit to capture such a signal. To further test this drawdown hypothesis, additional trace metal records are needed from several Ludfordian shale successions where the local redox conditions are consistently euxinic before, during, and after the LKE and associated Lau CIE to determine if these trends might represent global changes in trace metal inventories.

6. Conclusions

We have presented the first multi-proxy assessment of local paleo-redox variability in the Baltic Basin during the late Silurian (upper Gorstian–upper Ludfordian) from both shallow-shelf carbonate and deep-shelf shale/marl facies. Based on extremely low I/Ca values, the waters of the shallow shelf were influenced by consistently reducing marine waters via a significant exchange between the overlying water column and nearby reducing waters from a potential OMZ. Given the high Fe_{pyr}/Fe_{HR} values and moderately enriched trace metal concentrations, we suggest that the deep shelf of the Baltic Basin was dominated by a moderately-reducing, nitrogenous OMZ from the upper Gorstian through the lower/middle Ludfordian. The low Fe_{HR}/Fe_T suggest that there was no benthic iron shuttling from the shallow parts of the basin to the deep shelf, but the high Fe_{pyr}/Fe_{HR} values indicate the presence of sulfidic porewaters. It is likely that iron and sulfate reduction were happening exclusively within sediment porewaters in the upper Gorstian and lower Ludfordian. During the LKE interval, in the middle Ludfordian, there were notable coincident peaks in trace metal enrichments that may have been caused by a transient sulfidic event within the nitrogenous OMZ, briefly moving the sulfate reduction zone into the water column at the time when global marine redox conditions were the most reducing. These peaks were immediately followed by decreases in absolute trace metal concentration below UCC values during the rising limb of the Lau CIE, though TOC-normalized trace metal concentrations quickly rose back to concentrations similar to that of the early Ludfordian. Low Fe_{HR}/Fe_T and Fe_{pyr}/Fe_{HR} values, combined with variable trace metal concentrations, suggest that the sediments of the upper Ludfordian were deposited at or just below the basinward margin of the nitrogenous OMZ where redox conditions would have fluctuated.

The peak in trace metal enrichments in the initial stages of the LKE, just prior to the Lau CIE, corresponds to the early expansion of bottom water anoxia previously documented as a positive excursion in thallium isotopes from the same locality (Bowman et al., 2019). The sharp decrease in trace metal concentrations that follows during the rising limb of the Lau CIE and the parallel sulfur isotope excursion might represent an overprint of a global drawdown in trace metals due to the fraction of euxinic and sulfidic conditions in the global oceans expanding as organic carbon and pyrite burial increased globally (Bowman et al., 2019, 2020). To test this hypothesis, additional trace metal records are needed from other Ludfordian shale successions where the local redox conditions are consistently euxinic throughout the LKE and associated Lau CIE intervals.

This study highlights the utility of multi-proxy studies in understanding local paleo-redox change and variability during global events, such as Paleozoic CIEs and Mesozoic ocean anoxic events, using a suite of iodine, iron, and trace metal redox proxies to unravel the most probable water column and sediment pore-water redox conditions across the shelf. We have also demonstrated the importance of understanding local marine redox dynamics to then make possible links to global-ocean scale redox changes. This work is the first to constrain local redox conditions within the Baltic Basin from which the biotic record of the LKE is known in the greatest detail. Thus, we are able to tie together local records of extinction and faunal recovery to changes in local marine redox conditions in the late Silurian.

Declaration of Competing Interest

The authors declare that they have no known competing financial interests or personal relationships that could have appeared to influence the work reported in this paper.

Acknowledgments

Zunli Lu and one anonymous reviewer are thanked for their constructive reviews that helped to improve this paper and Tom Algeo for editorial direction. We thank N. Kozik and C. Richbourg for their assistance in sample processing and data collection and M. Calner for access to the Uddvide-1 core. This research was funded by the National Science Foundation (EAR-1748635 to SAY and JDO). This research was performed at the National High Magnetic Field Laboratory, which is supported by NSF Cooperative Agreement No. DMR-1644770 and the State of Florida.

Appendix A. Supplementary data

Supplementary data to this article can be found online at https://doi.org/10.1016/j.palaeo.2021.110624.

References

Algeo, T.J., Lyons, T.W., 2006. Mo-total organic carbon covariation iin modern anoxic marine environments: Implications for analysis of paleo redox and paleohydrographic conditions. Paleoceanogr. 21 (1), 1–23. https://doi.org/10.1029/2004PA001112.

Algeo, T.J., Maynard, J.B., 2004. Trace-element behavior and redox facies in core shales of Upper Pennsylvanian Kansas-type cyclothems. Chem. Geol. 206, 289–318. https://doi.org/10.1016/j.chemgeo.2003.12.009.

Algeo, T.J., Tribovillard, N., 2009. Environmental analysis of paleoceanographic systems based on molybdenum-uranium covariation. Chem. Geol. 268, 211–225. https://doi.org/10.1016/j.chemgeo.2009.09.001.

Amos, H.M., Jacob, D.J., Kocman, D., Horowitz, H.M., Zhang, Y., Dutkiewicz, S., Horvat, M., Corbitt, E.S., Krabbenhoft, D.P., Sunderland, E.M., 2014. Global biogeochemical implications of mercury discharges from rivers and sediment burial. Environ. Sci. Technol. 48 (16), 9514–9522. https://doi.org/10.1021/es502134t.

Bagnato, E., Oliveri, E., Acquavita, A., Covelli, S., Petranich, E., Barra, M., Italiano, F., Parello, F., Sprovieri, M., 2017. Hydrochemical mercury distribution and air-sea exchange over the submarine hydrothermal vents off-shore Panarea Island (Aeolian arc, Tyrrhenian Sea). Mar. Chem. 194, 63–78. https://doi.org/10.1016/j.marchem.2017.04.003.

Berner, R.A., 1970. Sedimentary pyrite formation. Am. J. Sci. 268 (1), 1–23. https://doi.org/10.2475/ajs.268.1.1.

Bond, D.P.G., Grasby, S.E., 2017. On the causes of mass extinctions. Palaeogeogr. Palaeoclimatol. Palaeoecol. 478, 3–29. https://doi.org/10.1016/j.palaeo.2016.11.005.

Bower, J., Savage, K.S., Weinman, B., Barnett, O.M., Hamilton, W.P., Harper, W.F., 2008. Immobilization of mercury by pyrite (FeS_2). Environ. Pollut. 156 (2), 504–514.

Bowman, C.N., Young, S.A., Kaljo, D., Eriksson, M.E., Them II, T.R., Hints, O., Martma, M., Owens, J.D., 2019. Linking the progressive expansion of reducing conditions to a stepwise mass extinction event in the late Silurian oceans. Geology 47 (10), 968–972. https://doi.org/10.1130/G46571.1.

Bowman, C.N., Lindskog, A., Kozik, N.P., Richbourg, C.G., Owens, J.D., Young, S.A., 2020. Integrated sedimentary, biotic, and paleoredox dynamics from multiple localities in southern Laurentia during the late Silurian (Ludfordian) extinction event. Palaeogeogr. Palaeoclimatol. Palaeoecol. 553, 109799. https://doi.org/10.1016/j.palaeo.2020.109799.

Boyer, D.L., Owens, J.D., Lyons, T.W., Droser, M.L., 2011. Joining forces: combined biological and geochemical high-resolution palaeo-oxygen history in Devonian epeiric seas. Palaeogeogr. Palaeoclimatol. Palaeoecol. 306, 134–146. https://doi.org/10.1016/j.palaeo.2011.04.012.

Brüchert, V., Jørgensen, B.B., Neumann, K., Riechmann, D., Schlösser, M., Schulz, H., 2003. Regulation of bacterial sulfate reduction and hydrogen sulfide fluxes in the central Namibian coastal upwelling zone. Geochim. Cosmochim. Acta 67, 4505–4518.

Calner, M., 2008. Silurian global events – At the tipping point of climate change. In: Elewa, A.M.T. (Ed.), Mass Extinctions. Springer-Verlag, Berlin, pp. 21–58.

Calvert, S.E., Pederson, T.F., 1993. Geochemistry of recent oxic and anoxic sediments: implications for the geological record. Mar. Geol. 113, 67–88.

Canfield, D.E., Berner, R.A., 1987. Dissolution and pyritization of magnetite in anoxic marine sediments. Geochim. Cosmochim. Acta 51, 645–659. https://doi.org/10.1016/0016-7037(87)90076-7.

Canfield, D.E., Thamdrup, B., 2009. Towards a consistent classification scheme for geochemical environments, or, why we wish the term 'suboxic' would go away. Geobiology 7, 385–392. https://doi.org/10.1111/j.1472-4669.2009.00214.x.

Canfield, D.E., Raiswell, R., Westrich, J.T., Reaves, C.M., Berner, R.A., 1986. The use of chromium reduction in the analysis of reduced inorganic sulfur in sediments and shales. Chem. Geol. 54, 149–155.

Canfield, D.E., Raiswell, R., Bottrell, S., 1992. The reactivity of sedimentary iron minerals toward sulfide. Am. J. Sci. 292, 659–683.

Canfield, D.E., Lyons, T.W., Raiswell, R., 1996. A model for iron deposition to euxinic Black Sea sediments. Am. J. Sci. 296 (7), 818–834. https://doi.org/10.2475/ajs.296.7.818.

del Rey, A., Havsteen, J.C., Bizarro, M., Dahl, T.W., 2020. Untangling the diagenetic history of uranium isotopes in marine carbonates: a case study tracing the $\delta^{238}U$ composition of late Silurian oceans using calcitic brachiopod shells. Geochim. Cosmochim. Acta 287, 93–110. https://doi.org/10.1016/j.gca.2020.06.002.

Dickens, G.R., Owen, R.M., 1994. Late Miocene-early Pliocene manganese redirection in the Central Indian Ocean: expansion of the intermediate water oxygen minimum zone. Paleoceanogr. 9 (1), 169–181.

Dickson, A.J., Jenkyns, H.C., Porcelli, D., van den Boorn, S., Idiz, E., Owens, J.D., 2016. Corrigendum to "Basin-scale controls on the molybdenum-isotope composition of seawater during Ocean Anoxic Event 2 (Late Cretaceous)". Geochim. Cosmochim. Acta 189, 404–405. https://doi.org/10.1016/j.gca.2016.06.025.

Eriksson, M.J., Calner, M., 2008. A sequence stratigraphical model for the late Ludfordian (Silurian) of Gotland, Sweden: implications for timing between changes in sea level, palaeoecology, and the global carbon cycle. Facies 54, 253–276. https://doi.org/10.1007/s10347-007-0128-y.

Force, E.R., Cannon, W.F., 1988. Depositional model for shallow-marine manganese deposits around black shale basins. Econ. Geol. 83, 93–117.

Force, E.R., Maynard, J.B., 1991. Manganese: Syngenetic deposits on the margins of anoxic basins. Rev. Econ. Geol. 5, 147–160.

Froelich, P.N., Klinkhammer, G.P., Bender, M.L., Luedtke, N.A., Heath, G.R., Cullen, D., Dauphin, P., Hammond, D., Hartman, B., Maynard, V., 1979. Early oxidation of organic matter in pelagic sedimetns of the eastern equatorial Atlantic: suboxic diagenesis. Geochim. Cosmochim. Acta 43 (7), 1075–1090. https://doi.org/10.1016/0016-7037(79)90095-4.

Fryda, J., Lehnert, O., Frydova, B., Farkaš, J., Kubajko, M., 2021. Carbon and sulfur cycling during the mid-Ludfordian anomaly and the linkage with the late Silurian Lau/Kozlowskii Bioevent. Palaeogeogr. Palaeoclimatol. Palaeoecol. 564, 110152. https://doi.org/10.1016/j.paleo.2020.110152.

Gill, B.C., Lyons, T.W., Jenkyns, H.C., 2011. A global perturbation to the sulfur cycle during the Toarcian Oceanic Anoxic Event. Earth Planet. Sci. Lett. 312, 484–496. https://doi.org/10.1016/j.epsl.2011.10.030.

Grasby, S.E., Them II, T.R., Chen, Z., Yin, R.S., Ardakani, O.H., 2019. Mercury as a proxy for volcanic emissions in the geologic record. Earth-Sci. Rev. 196, 102880. https://doi.org/10.1016/j.earscirev.2019.102880.

Gruber, N., Sarmiento, J.L., 1997. Global patterns of marine nitrogen fixation and denitrification. Glob. Biogeochem. Cycles 11, 235–266.

Hammersley, M.R., Lavik, G., Woebken, D., Rattray, J.E., Lam, P., Hopmans, E.C., Damste, J.S.S., Kruger, S., Graco, M., Gutierrez, D., Kuypers, M.M.M., 2007. Anaerobic ammonium oxidation in the Peruvian oxygen minimum zone. Limnol. Oceanogr. 52, 923–933.

Hardisty, D.S., Lu, Z., Planavsky, N.J., Bekker, A., Philippot, P., Zhou, X., Lyons, T.W., 2014. An iodine record of Paleoproterozoic surface ocean oxygenation. Geology 42 (2), 619–622. https://doi.org/10.1130/G35439.1.

Hardisty, D.S., Lu, Z., Bekker, A., Diamond, C.W., Gill, B.C., Jiang, G., Kah, L.C., Knoll, A. H., Loyd, S.J., Osburn, M.R., Planavsky, N.J., Wang, C., Zhou, X., Lyons, T.W., 2017. Perspectives on Proterozoic surface ocean redox from iodine contents in ancient and recent carbonate. Earth Planet. Sci. Lett. 463, 159–170. https://doi.org/10.1016/j.epsl.2017.01.032.

Hardisty, D.S., Lyons, T.W., Riedinger, N., Isson, T.T., Owens, J.D., Aller, R.C., Rye, D.M., Planavsky, N.J., Reinhard, C.T., Gill, B.C., Masterson, A.L., Asael, D., Johnston, D.T., 2018. An Evaluation of Sedimentary Molybdenum and Iron as Proxies for Pore Fluid Paleoredox Conditions. Am. J. Sci. 318, 527–556. https://doi.org/10.2475/05.2018.04.

Hardisty, D.S., Horner, T.J., Evans, N., Moriyasu, R., Babbin, A.R., Wankel, S.D., Moffett, J.W., Nielsen, S.G., 2021. Limited iodate reduction in shipboard seawater incubations from the Eastern Tropical North Pacific oxygen deficient zone. Earth Planet. Sci. Lett. 554, 116676. https://doi.org/10.1016/j.epsl.2020.116676.

Jeppsson, L., 1983. Silurian conodont faunas from Gotland. Foss. Strat. 15, 121–144.

Jeppsson, L., 1990. An oceanic model for lithological and faunal changes tested on the Silurian record. J. Geol. Soc. Lond. 147, 663–674.

Jeppsson, L., 2005. Conodont-based revisions of the late Ludfordian on Gotland, Sweden. GFF 127, 273–282. https://doi.org/10.1080/11035890501274273.

Kaljo, D., Martma, T., 2006. Application of carbon isotope stratigraphy to dating the Baltic Silurian rocks. GFF 128, 123–129. https://doi.org/10.1080/11035890601282123.

Kaljo, D., Kiipli, T., Martma, T., 1997. Carbon isotope event markers through the Wenlock-Pridoli sequence at Ohesaare (Estonia) and Priekule (Latvia). Palaeogeogr. Palaeoclimatol. Palaeoecol. 132, 211–223.

Kiipli, T., Kiipli, E., Kaljo, D., 2010. Silurian Sea level variations estimated using SiO_2/Al_2O_3 and K_2O/Al_2O_3 ratios in the Priekule drill core section, Latvia. Bull. Paleontol. Soc. Italy 41 (1), 55–63.

Koren, T.N., 1993. Main event levels in the evolution of the Ludlow graptolites. Geol. Correl. 1, 44–52.

Kozłowski, W., Munnecke, A., 2010. Stable carbon isotope development and sea-level changes during the late Ludlow (Silurian) of the Łysogóry region (Rzepin section, Holy Cross Mountains, Poland). Facies 56, 615–633. https://doi.org/10.1007/s10347-010-0220-6.

Kozłowski, W., Sobień, K., 2012. Mid-Ludfordian coeval carbon isotopes, natural gamma ray and magnetic susceptibility excursions in Mielnik IG-1 borehole (Eastern Poland)—Dustiness as a possible link between global climate and the Silurian carbon isotope record. Palaeogeogr. Palaeoclimatol. Palaeoecol. 339-341, 74–97. https://doi.org/10.1016/j.palaeo.2012.04.024.

Kuypers, M.M.M., Lavik, G., Woebken, D., Schmid, M., Fuchs, B.M., Amann, R., Jørgensen, B.B., Jetten, M.S.M., 2005. Massive nitrogen loss from the Benguela upwelling system through anaerobic ammonium oxidation. Proc. Natl. Acad. Sci. 102, 6478–6483.

Lam, P., Kuypers, M.M.M., 2011. Microbial nitrogen cycling processes in oxygen minimum zones. Annu. Rev. Mar. Sci. 3, 317–345.

Lau, K.V., Maher, K., Altiner, D., Kelley, B.M., Kump, L.R., Lehrmann, D.J., Silva-Tamayo, J.C., Weaver, K.L., Yu, M., Payne, J., 2016. Marine anoxia and delayed Earth system recovery after the end-Permian extinction. Proc. Natl. Acad. Sci. 113 (9), 2360–2365. https://doi.org/10.1073/pnas.1515080113.

Lau, K.V., Romaniello, S.J., Zhang, F., 2019. The Uranium Isotope Paleoredox Proxy. In: Lyons, T.W., Turchyn, A., Reinhard, C. (Eds.), Cambridge Elements: Geochemical Tracers in Earth System Science. Cambridge University Press, Cambridge. https://doi.org/10.1017/9781108731119.

Lehnert, O., Fryda, J., Buggisch, W., Munnecke, A., Nützel, A., Križ, J., Manda, S., 2007. $\delta^{13}C$ records across the late Silurian Lau event: New data from middle palaeolatitudes of northern peri-Gondwana (Prague Basin, Czech Republic). Palaeogeogr. Palaeoclimatol. Palaeoecol. 245, 227–244. https://doi.org/10.1016/j.palaeo.2006.02.022.

Lu, Z., Jenkyns, H.C., Rickaby, R.E.M., 2010. Iodine to calcium ratios in marine carbonate as a paleoredoxproxy during oceanic anoxic events. Geology 38 (12), 1107–1110. https://doi.org/10.1130/G31145.1.

Lu, Z., Hoogakker, B.A.A., Hillenbrand, C.-D., Zhou, X., Thomas, E., Gutchess, K.M., Lu, W., Jones, L., Rickaby, R.E.M., 2016. Oxygen depletion recorded in upper waters of the glacial Southern Ocean. Nat. Commun. 7, 1–8. https://doi.org/10.1038/ncomms11146.

Lu, W., Wörndle, S., Halverson, G.P., Zhou, X., Bekker, A., Rainbird, R.H., Hardisty, D.S., Lyons, T.W., Lu, Z., 2017. Iodine proxy evidence for increased ocean oxygenation during the Bitter Springs Anomaly. Geochem. Perspect. Lett. 5, 53–57. https://doi.org/10.7185/geochemlet.1746.

Lu, W., Ridgwell, A., Thomas, E., Hardisty, D.S., Luo, G., Algeo, T.J., Saltzman, M.R., Gill, B.C., Shen, Y., Ling, H., Edwards, C.T., Whalen, M.T., Zhou, X., Gutchess, K.M., Jin, L., Rickaby, R.E.M., Jenkyns, H.C., Lyons, T.W., Lenton, T.M., Kump, L.R., Lu, Z., 2018. Late inception of a resiliently oxygenated upper ocean. Science 361, 174–177. https://doi.org/10.1126/science.aar5372.

Lu, W., Dickson, A.J., Thomas, E., Rickaby, R.E.M., Chapman, P., Lu, Z., 2019. Refining the planktic foramniferal I/Ca proxy: results from the Southeast Atlantic Ocean. Geochim. Cosmochim. Acta 287, 318–327. https://doi.org/10.1016/j.gca.2019.10.025.

Lyons, T.W., Kashgarian, M., 2005. Paradigm lost, paradigm found. Oceanography 18, 86–99. https://doi.org/10.5670/oceanog.2005.44.

Lyons, T.W., Severmann, S., 2006. A critical look at iron paleoredox proxies: New insights from modern euxinic marine basins. Geochim. Cosmochim. Acta 70 (23), 5698–5722. https://doi.org/10.1016/j.gca.2006.08.021.
Manda, S., Štorch, P., Slavík, L., Fryda, J., Kríž, J., Tasáryová, A., 2012. The graptolite, conodont and sedimentary record through the late Ludlow Kozlowskii Event (Silurian) in the shale-dominated succession of Bohemia. Geol. Mag. 149 (3), 507–531. https://doi.org/10.1017/S0016756811000847.
März, C., Poulton, S.W., Beckman, B., Küster, K., Wagner, T., Kasten, S., 2008. Redox sensitivity of P cycling during marine black shale formation: Dynamics of sulfidic and anoxic, non-sulfidic bottom waters. Geochim. Cosmochim. Acta 72 (15), 3703–3717. https://doi.org/10.1016/j.gca.2008.04.025.
McLennan, S.M., 2001. Relationships between the trace element composition of sedimentary rocks and upper continental crust. Geochem. Geophys. Geosyst. 2 (4) https://doi.org/10.1029/2000GC000109.
Miller, C.A., Peucker-Ehrenbrink, B., Walker, B.D., Marcatonio, F., 2011. Re-assessing the surface cycling of molybdenum and rhenium. Geochim. Cosmochim. Acta 75 (22), 77146–77179. https://doi.org/10.1016/j.gca.2011.09.005.
Morford, J.L., Emerson, S., 1999. The geochemistry of redox sensitive trace metals in sediments. Geochim. Cosmochim. Acta 63 (11–12), 1735–1750.
Morford, J.L., Russel, A.D., Emerson, S., 2001. Trace metal evidence for changes in the redox environment associated with the transition from terrigenous clay to diatomaceous sediments, Saanich Inlet. BC. Mar. Geol. 174, 355–369.
Munnecke, A., Samtleben, C., Bickert, T., 2003. The Ireviken Event in the lower Silurian of Gotland, Sweden – relation to similar Palaeozoic and Proterozoic events. Palaeogeogr. Palaeoclimatol. Palaeoecol. 195, 99–124. https://doi.org/10.1016/S0031-0182(03)00304-3.
Nehring-Lefeld, M., Modliński, Z., Swadowska, E., 1997. Thermal evolution of the Ordovician in the western margin of the East-European Platform: CAI and Ro data. Geol. Q. 41 (2), 129–138.
Owens, J.D., 2019. Application of Thallium Isotopes. In: Lyons, T.W., Turchyn, A., Reinhard, C. (Eds.), Elements in Geochemical Tracers in Earth System Science. Cambridge University Press, Cambridge. https://doi.org/10.1017/9781108688697.
Owens, J.D., Gill, B.C., Jenkyns, H.C., Bates, S.M., Severmann, S., Kuypers, M.M.M., Woodfine, R.G., Lyons, T.W., 2013. Sulfur isotopes track the global extent and dynamics of euxinia during cretaceous Oceanic Anoxic Event 2. Proc. Natl. Acad. Sci. 110, 18407–18412. https://doi.org/10.1073/pnas.1305304110.
Owens, J.D., Reinhard, C.T., Rohrssen, M., Love, G.D., Lyons, T.W., 2016. Empirical links between trace metal cycling and marine microbial ecology during a large perturbation to Earth's carbon cycle. Earth Planet. Sci. Lett. 449, 407–417. https://doi.org/10.1016/j.epsl.2016.05.046.
Owens, J.D., Lyons, T.W., Hardisty, D.S., Lowery, C.M., Lu, Z., Lee, B., Jenkyns, H.C., 2017. Patterns of local and global redox variability during the Cenomanian-Turonian Boundary Event (Ocean Anoxic Event 2) recorded in carbonates and shales from Central Italy. Sedimentology 64, 168–185. https://doi.org/10.1111/sed.12352.
Poulton, S.W., Canfield, D.E., 2005. Development of a sequential extraction procedure for iron: implications for iron partitioning in continentally derived particulates. Chem. Geol. 214, 209–221.
Poulton, S.W., Canfield, D.E., 2011. Ferruginous Conditions: a dominant feature of the ocean through Earth's history. Elements 7, 107–112.
Raiswell, R., Canfield, D.E., 1998. Sources of iron for pyrite formation in marine sediments. Am. J. Sci. 298 (3), 219–245. https://doi.org/10.2475/ajs.298.3.219.
Raiswell, R., Newton, R., Bottrell, S.H., Coburn, P.M., Briggs, D.E.G., Bond, D.P.G., Poulton, S.W., 2008. Turbidite depositional influences on the diagenesis of Beecher's Trilobite Bed and the Hunsruck Slate: Sites of soft tissue pyritization. Am. J. Sci. 308, 105–129. https://doi.org/10.2475/02.2008.01.
Raiswell, R., Hardisty, D.S., Lyons, T.W., Canfield, D.E., Owens, J.D., Planavsky, N.J., Poulton, S.W., Reinhard, C.T., 2018. The iron paleoredox proxies: a guide to the pitfalls, problems and proper practice. Am. J. Sci. 318, 491–526. https://doi.org/10.2475/05.2018.03.
Rudnick, R.L., Gao, S., 2003. 3.01 - Composition of the Continental Crust. In: Holland, H., Turekian, K. (Eds.), Treatise on Geochemistry, 1st edition. Elsevier, Oxford, pp. 1–64. https://doi.org/10.1016/B0-08-043751-6/03016-4.
Rudnick, R.L., Gao, S., 2014. 4.1 – Composition of the Continental Crust. In: Turekian, K., Holland, H. (Eds.), Treatise on Geochemistry, 2nd edition. Elsevier, Oxford, pp. 1–51.
Rue, E.L., Smith, G.J., Cutter, G.A., Bruland, K.W., 1997. The response of trace element redox couples to suboxic conditions in the water column. Deep-Sea Res. I 44 (1), 113–134.
Sadler, P.M., 1981. Sediment accumulation rates and the completeness of stratigraphic sections. J. Geol. 89, 569–584.
Saltzman, M.R., Thomas, E., 2012. Carbon Isotope Stratigraphy, in: Goldstein, F.M., Ogg, J. G., Schmitz, M. (Eds.). Geologic Time Scale 2012, 207–267. https://doi.org/10.1016/B978-0-444-59425-9.00011-1.
Sanei, H., Grasby, S.E., Beauchamp, B., 2012. Latest Permian mercury anomalies. Geology 40 (1), 63–66. https://doi.org/10.1130/G32596.1.
Schnuck, H., Lavik, G., Desai, D.K., Grosskopf, T., Kalvelage, T., Loescher, C.R., Paulmier, A., Contreras, S., Siegel, H., Holtappels, M., Rosential, P., Schilhabel, M.B., Graco, M., Schmitz, R.A., Kuypers, M.M.M., LaRoche, J., 2013. Giant hydrogen sulfide plume in the oxygen minimum zone off Peru supports chemolithoautotrophy. PLoS One 8 (8), e68661. https://doi.org/10.1371/journal.pone.0068661.
Scholz, F., 2018. Identifying oxygen minimum zone-type biogeochemical cyclng in Earth history using inorganic geochemical proxies. Earth-Sci. Rev. 184, 29–45. https://doi.org/10.1016/j.earscirev.2018.08.002.
Scholz, F., Hensen, C., Noffke, A., Rohde, A., Liebetrau, V., Wallmann, K., 2011. Early diagenesis of redox-sensitive trace metals in the Peru upwelling area: response to ENSO-related oxygen fluctuations in the water column. Geochim. Cosmochim. Acta 75, 7257–7276.
Scholz, F., McManus, J., Mix, A.C., Hensen, C., Schneider, R.R., 2014. The impact of ocean deoxygenation on iron release from continental margin sediments. Nat. Geosci. 7, 433–437. https://doi.org/10.1038/ngeo2162.
Scholz, F., Löscher, C.R., Fiskal, A., Sommer, S., Hensen, C., Lomnitz, U., Wuttig, K., Göttlicher, J., Kossel, E., Steininger, R., Canfield, D.E., 2016. Nitrate-dependent iron oxidation limits iron transport in anoxic ocean regions. Earth Planet. Sci. Lett. 454, 272–281. https://doi.org/10.1016/j.epsl.2016.09.025.
Scott, C., Lyons, T.W., 2012. Contrasting molybdenum cycling and isotopic properties in euxinic versus non-euxinic sediments and sedimentary rocks: refining the paleoproxies. Chem. Geol. 324-325, 19–27. https://doi.org/10.1016/j.chemgeo.2012.05.012.
Shen, J., Algeo, T.J., Chen, J., Planavsky, N.J., Feng, Q., Yu, J., Liu, J., 2019. Mercury in marine Ordovician/Silurian boundary sections of South China is sulfide-hosted and non-volcanic in origin. Earth Planet. Sci. Lett. 511, 130–140. https://doi.org/10.1016/j.epsl.2019.01.028.
Shen, J., Feng, Q., Algeo, T.J., Liu, J., Zhou, C., Wei, W., Liu, J., Them II, T.R., Gill, B.C., Chen, J., 2020. Sedimentary host phases of mercury (Hg) and implications for their use as a volcanic proxy. Earth Planet. Sci. Lett. 543, 116333. https://doi.org/10.1016/j.epsl.2020.116333.
Stricanne, L., Munnecke, A., Pross, J., 2006. Assessing mechanisms of environmental change: Palynological signals across the late Ludlow (Silurian) positive isotope excursion ($\delta^{13}C$, $\delta^{18}O$) on Gotland, Sweden. Palaeogeogr. Palaeoclimatol. Palaeoecol. 230, 1–31. https://doi.org/10.1016/j.palaeo.2005.07.003.
Them II, T.R., Jagoe, C.H., Caruthers, A.H., Gill, B.C., Grasby, S.E., Gröcke, D.R., Yin, R. S., Owens, J.D., 2019. Terrestrial sources as the primary delivery mechanism of mercury to the oceans across the Toarcian Oceanic Anoxic Event (early Jurassic). Earth Planet. Sci. Lett. 507, 62–72. https://doi.org/10.1016/j.epsl.2018.11.029.
Tribovillard, N., Algeo, T.J., Lyons, T.W., Riboleau, A., 2006. Trace metals as paleoredox and paleoproductivity proxies: an update. Chem. Geol. 232, 12–32. https://doi.org/10.1016/j.chemgeo.2006.02.012.
Turgeon, S., Brumsack, H.J., 2006. Anoxic vs dysoxic events reflected in sedimentary geochemistry during the Cenomanian-Turonian Boundary Event (cretaceous) in the Umbria-Marche Basin of Central Italy. Chem. Geol. 234, 321–339. https://doi.org/10.1016/j.chemgeo.2006.05.008.
Urbanek, A., 2003. Biotic crises in the history of the upper Silurian graptoloids: a paleobiological model. Hist. Biol. 7, 29–50.
Younes, H., Calner, M., Lehnert, O., 2017. The first continuous $\delta^{13}C$ record across the late Silurian Lau Event on Gotland, Sweden. GFF 139, 63–69. https://doi.org/10.1080/11035897.2016.1227362.
Young, S.A., Kleinberg, A., Owens, J.D., 2019. Geochemical evidence for expansion of marine euxinia during an early Silurian (Llandovery-Wenlock boundary) mass extinction. Earth Planet. Sci. Lett. 513, 1187–1196. https://doi.org/10.1016/j.epsl.2019.02.023.
Young, S.A., Benayoun, E., Kozik, N.P., Hints, O., Martma, T., Bergström, S.M., Owens, J. D., 2020. Marine redox variability from Baltica during extinction events in the latest Ordovician-early Silurian. Palaeogeogr. Palaeoclimatol. Palaeoecol. 553, 109792. https://doi.org/10.1016/j.palaeo.2020.109792.
Zhang, F., Romaniello, S.J., Algeo, T.J., Lau, K.V., Clapham, M.E., Richoz, S., Herrmann, A.D., Smith, H., Horacek, M., Anbar, A.D., 2018. Multiple episodes of extensive marine anoxia linked to global warming and continental weathering following the latest Permian mass extinction. Sci. Adv. 4, e1602921 https://doi.org/10.1126/sciadv.1602921.
Zhou, X., Thomas, E., Rickaby, R.E.M., Winguth, A.M.E., Lu, Z., 2014. I/Ca evidence for upper ocean deoxygenation during the PETM. Paleoceanogr. 29, 1–12. https://doi.org/10.1002/2014PA002702.
Zhou, X., Jenkyns, H.C., Owens, J.D., Junium, C.K., Zheng, X.-Y., Sageman, B.B., Hardisty, D.S., Lyons, T.W., Ridgewell, A., Lu, Z., 2015. Upper Ocean oxygenation dynamics from I/Ca ratios during the Cenomanian-Turonian OAE 2. Paleoceanogr. 30, 510–526. https://doi.org/10.1002/2014PA002741.